JOURNAL OF COMPUTATIONAL PHYSICS 106, 306–318 (1993)

A Coupled Implicit Method for Chemical Non-equilibrium Flows at All Speeds

JIAN-SHUN SHUEN

Sverdrup Technology, Inc., NASA Lewis Research Center, Cleveland, Ohio 44135

KUO-HUEY CHEN

University of Toledo, NASA Lewis Research Center, Cleveland, Ohio 44135

AND

YUNHO CHOI

Sverdrup Technology, Inc., NASA Lewis Research Center, Cleveland, Ohio 44135

Received January 13, 1992

A time-accurate, coupled solution procedure is described for the chemical nonequilibrium Navier–Stokes equations over a wide range of Mach numbers. This method employs the strong conservation form of the governing equations, but uses primitive variables (ρ_g, u, v, h, Y_i) as unknowns. Real gas properties and nonequilibrium chemistry are considered. Numerical tests include steady convergent–divergent nozzle flows with air dissociation/recombination chemistry, dump combustor flows with n-pentane–air chemistry, and nonreacting unsteady driven cavity flows. Numerical results for both the steady and unsteady flows demonstrate the efficiency and robustness of the present algorithm for Mach numbers ranging from the incompressible limit to supersonic speeds.

1. INTRODUCTION

The computation of the flow involving wide variations in Mach number often poses problems for contemporary compressible flow algorithms. Chemically reacting flow in an aeropropulsion system is a typical example of such cases. The characteristic trait of this flow is that the fluid velocity in a large portion of the computational domain is much smaller than the acoustic speed, and yet the density variation is significant or the flow velocity in other parts of the domain may be large so as to preclude an incompressible approach. Other examples of such flows of interest include large embedded recirculation zones in an otherwise high-speed flow, flow in a large contraction ratio convergent–divergent nozzle, and rocket motor flow in which the Mach number is zero at the closed end of the chamber and supersonic at the nozzle exit. The difficulties are primarily in the computation of the low speed regions of the flow [1–5].

Numerical algorithms developed for compressible flows are often ineffective at low Mach numbers. There are two well-recognized reasons [1–5] for this difficulty. First, the system's eigenvalues become stiff at low flow velocities. In theory, this can be circumvented by using a large CFL number in implicit schemes. In practice, however, a large approximate factorization error in multidimensions introduces the optimum CFL number beyond which convergence slows down. At low Mach numbers, there are large disparities among CFL numbers based on each eigenvalue and the numbers cannot become the same optimum number simultaneously. Second, the pressure term in the momentum equations becomes singular as the Mach number approaches zero, yielding a large roundoff error. This behavior smears the pressure variation field and often produces inaccurate solutions.

In many important physical problems (e.g., thermally driven flow, laminar diffusion flame, liquid droplet vaporization), Mach numbers as low as 10^{-7} are of interest. To solve flows in this Mach number range, perturbation expansion techniques have been developed by Merkle and Choi [4], Oran and Boris [6], and Guerra and Gustafsson [7]. The method is based on the expansion of flow variables in a small parameter proportional to Mach number squared [4, 6] or Mach number [7]. The result is an approximate set of equations valid only at low Mach numbers, but which has well-conditioned pressure gradient terms in the momentum equations as well as a set of well-conditioned eigenvalues. Rapid and uniform convergence rates for Mach numbers from 10^{-1} to 10^{-5} were observed in [4]. The major deficiency of this approach is that it is not valid at moderate and high speeds.

Recently, Patnaik *et al.* [8] extended the flux-correct

0021-9991/93 $5.00

transport (FCT) scheme discussed in [6] to low Mach number flows using a predictor–corrector procedure. In [8], an implicit correction step for solving one elliptic pressure correction equation was added to the baseline explicit FCT method (predictor). The resulting scheme was applied to nonreacting flows for Mach numbers as low as 0.03 with good computational efficiency. Ramshaw *et al.* [9] reported a pressure gradient scaling (PGS) method for low Mach number flow with nearly uniform spatial pressure field. The PGS method suffers from the same deficiency as the perturbation method, i.e., it is not valid at moderate and high Mach numbers.

There are many physical problems in which the bulk flow velocity varies from near zero to supersonic, and therefore it would be necessary to use a numerical algorithm which is effective for a wide range of Mach numbers. In this regard, preconditioning methods [1–3] have received considerable attention and demonstrated their effectiveness for certain classes of flow problems. The preconditioning approach involves premultiplying the time derivative terms in the governing equations by a matrix designed to rescale the system's eigenvalues. Earlier studies [1, 2] showed that, with preconditioning, identical rates of convergence could be obtained for Mach numbers from 0.05 to 0.7. However, this approach is not adequate below Mach number 0.01, since control of roundoff error was not considered. Moreover, the above results were limited to inviscid flows.

Recently, Choi and Merkle [5] reported a new preconditioning procedure for ideal gas flows at all speeds for both inviscid and viscous cases. Their method has well-conditioned eigenvalues and pressure gradient terms for all Mach numbers and Reynolds numbers and therefore represents a very promising approach in the pursuit of an all speed algorithm. In addition, Chen and Pletcher [10] developed a strongly implicit procedure intended for flows with a wide Mach number range. Results in [10] showed that the method yielded fast convergence for Mach numbers from 0.05 to transonic. Since the set of governing equations still has ill-conditioned eigenvalues as well as the pressure singularity problem, the procedure in [10] might become less effective for Mach numbers below 0.01.

Chemically reacting flows exhibit another category of numerical difficulties because of the wide range of time scales involved in their calculation. To avoid this stiffness problem, chemical source terms are usually treated implicitly. This measure is equivalent to preconditioning the time derivative terms of the species conservation equations so that all chemical and convective processes proceed at approximately the same numerical rate. Although a number of reacting flow algorithms for high-speed flows have been developed in the past few years [11–13], chemical reactions have not been considered in most of the low-speed compressible flow algorithms, with a notable exception of [14]. In Ref. [14], a semi-implicit predictor–corrector procedure was used to solve the chemical nonequilibrium flow equations at low speed. Similar to the SIMPLE algorithm, the discretized equations were solved in a decoupled, sequential manner. Hosangadi *et al.* [15] recently reported a study in which the method in [4] was extended to consider combustion in low Mach number flows. However, because of the adoption of the flame sheet model (infinite reaction rate) and the simplifying assumptions used in the treatment of thermodynamic and transport properties, their method is not generally applicable to most combustion problems.

The objective of this study is to develop a unified solution algorithm for calculating chemical nonequilibrium flows at all Mach numbers, ranging from molecular diffusion velocity to supersonic speeds. Finite-rate chemistry and real-gas thermophysical properties are considered in the analysis. The approach we adopted here is an extension and refinement of the method in [5] for nonreacting ideal gas flows. Numerical test cases considered include convergent–divergent nozzle flows with air dissociation/recombination chemistry, dump combustor flows with a hydrocarbon fuel (*n*-pentane)–air reaction chemistry, and nonreacting unsteady driven cavity flows.

2. MATHEMATICAL FORMULATION

2.1. *Governing Equations*

The unsteady compressible Navier–Stokes and species transport equations for a chemically reacting gas of N species written in general curvilinear coordinates can be expressed as

$$\frac{\partial \tilde{\mathbf{Q}}}{\partial t}+\frac{\partial(\tilde{\mathbf{E}}-\tilde{\mathbf{E}}_v)}{\partial \xi}+\frac{\partial(\tilde{\mathbf{F}}-\tilde{\mathbf{F}}_v)}{\partial \eta}=\tilde{\mathbf{H}}, \tag{1}$$

where the vectors $\tilde{\mathbf{Q}}$, $\tilde{\mathbf{E}}$, $\tilde{\mathbf{F}}$, $\tilde{\mathbf{E}}_v$, $\tilde{\mathbf{F}}_v$, and $\tilde{\mathbf{H}}$ are defined as

$$\tilde{\mathbf{Q}}=\frac{y^\delta}{J}\mathbf{Q},$$

$$\tilde{\mathbf{E}}=\frac{y^\delta}{J}(\xi_t\mathbf{Q}+\xi_x\mathbf{E}+\xi_y\mathbf{F}),$$

$$\tilde{\mathbf{F}}=\frac{y^\delta}{J}(\eta_t\mathbf{Q}+\eta_x\mathbf{E}+\eta_y\mathbf{F}),$$

$$\tilde{\mathbf{E}}_v=\frac{y^\delta}{J}(\xi_x\mathbf{E}_v+\xi_y\mathbf{F}_v),$$

$$\tilde{\mathbf{F}}_v=\frac{y^\delta}{J}(\eta_x\mathbf{E}_v+\eta_y\mathbf{F}_v),$$

$$\tilde{\mathbf{H}}=\frac{1}{J}\mathbf{H}.$$

In the above expressions, t, ξ, and η are the time and spatial coordinates in generalized coordinates and ξ_t and η_t are the

grid speed terms. The ξ_x, ξ_y, η_x, and η_y are the metric terms and the J is the transformation Jacobian. The power, δ, is an index for two types of governing equations with $\delta = 0$ for two-dimensional and $\delta = 1$ for axisymmetric cases (with x being the axial and y the radial coordinates, respectively). The vectors $\mathbf{Q}$, $\mathbf{E}$, $\mathbf{F}$, $\mathbf{E}_v$, and $\mathbf{F}_v$ in the above definitions are

$$\mathbf{Q} = (\rho, \rho u, \rho v, \rho E, \rho Y_1, ..., \rho Y_{N-1})^T,$$

$$\mathbf{E} = (\rho u, \rho u^2 + p, \rho uv, (\rho E + p)u, \rho u Y_1, ..., \rho u Y_{N-1})^T,$$

$$\mathbf{F} = (\rho v, \rho uv, \rho v^2 + p, (\rho E + p)v, \rho v Y_1, ..., \rho v Y_{N-1})^T,$$

$$\mathbf{E}_v = (0, \tau_{xx}, \tau_{xy}, u\tau_{xx} + v\tau_{xy} + q_{x_e}, q_{x_1}, ..., q_{x_{N-1}})^T$$

$$\mathbf{F}_v = (0, \tau_{xy}, \tau_{yy}, u\tau_{xy} + v\tau_{yy} + q_{y_e}, q_{y_1}, ..., q_{y_{N-1}})^T,$$

and the source term vector $\mathbf{H}$ is

$$\mathbf{H} = \begin{bmatrix} 0 \\ -\frac{2}{3}\delta\left(\xi_x \frac{\partial \mu v}{\partial \xi} + \eta_x \frac{\partial \mu v}{\partial \eta}\right) \\ \delta\left[p - \frac{4}{3}\frac{\mu v}{y} + \frac{2}{3}\mu\left(\xi_x \frac{\partial u}{\partial \xi} + \eta_x \frac{\partial u}{\partial \eta}\right) - \frac{2}{3}v\left(\xi_y \frac{\partial \mu}{\partial \xi} + \eta_y \frac{\partial \mu}{\partial \eta}\right)\right] \\ -\frac{2}{3}\delta\left(\xi_x \frac{\partial \mu u v}{\partial \xi} + \eta_x \frac{\partial \mu u v}{\partial \eta} + \xi_y \frac{\partial \mu v^2}{\partial \xi} + \eta_y \frac{\partial \mu v^2}{\partial \eta}\right) \\ y^\delta S_1 \\ \vdots \\ y^\delta S_{N-1} \end{bmatrix},$$

where, ρ, p, u, and v represent the density, pressure, and Cartesian velocity components; $E = e + \frac{1}{2}(u^2 + v^2)$ is the total internal energy with e being the thermal internal energy; Y_i is the mass fraction of species i; and S_i is the rate of change of species i due to chemical reactions. The normal and shear stresses, and energy and species diffusion fluxes are given by

$$\tau_{xx} = 2\mu \frac{\partial u}{\partial x} - \frac{2}{3}\mu\left(\frac{\partial u}{\partial x} + \frac{\partial v}{\partial y}\right),$$

$$\tau_{xy} = \mu\left(\frac{\partial u}{\partial y} + \frac{\partial v}{\partial x}\right),$$

$$\tau_{yy} = 2\mu \frac{\partial v}{\partial y} - \frac{2}{3}\mu\left(\frac{\partial u}{\partial x} + \frac{\partial v}{\partial y}\right),$$

$$q_{x_e} = k\frac{\partial T}{\partial x} + \rho \sum_{i=1}^{N} h_i D_{im} \frac{\partial Y_i}{\partial x},$$

$$q_{y_e} = k\frac{\partial T}{\partial y} + \rho \sum_{i=1}^{N} h_i D_{im} \frac{\partial Y_i}{\partial y},$$

$$q_{x_i} = \rho D_{im} \frac{\partial Y_i}{\partial x},$$

$$q_{y_i} = \rho D_{im} \frac{\partial Y_i}{\partial y},$$

where T, μ, and k are the temperature, viscosity, and thermal conductivity, respectively; $D_{im} = (1 - X_i)/\sum_{j \neq i}^{N} X_j/D_{ij}$ is the effective binary diffusivity of species i in the gas mixture, X_i the molar fraction of species i, and D_{ij} the binary mass diffusivity between species i and j.

With the conventional compressible flow numerical algorithms the temperature and pressure are calculated iteratively from the equations [11, 16]

$$e = \sum_{i=1}^{N} Y_i h_i - \frac{p}{\rho}, \qquad h_i = h_{f_i}^\circ + \int_{T_{\text{ref}}}^{T} C_{p_i}\, dT,$$
$$p = \rho R_u T \sum_{i=1}^{N} \frac{Y_i}{W_i}, \tag{2}$$

where R_u and T_{ref} are the universal gas constant and reference temperature for thermodynamic properties, and W_i, C_{p_i}, h_i, $h_{f_i}^\circ$ are the molecular weight, constant pressure specific heat, thermodynamic enthalpy, and heat of formation of species i, respectively.

In reacting flow calculations, the evaluation of thermophysical properties is of vital importance. In this paper, the values of C_p, k, and μ for each species are determined by fourth-order polynominals of temperature, as described in [16]. The specific heat of the gas mixture is obtained by mass concentration weighting of individual species. The thermal conductivity and viscosity of the mixture, however, are calculated using Wilke's mixing rule [17]. The binary mass diffusivity D_{ij} between species i and j is obtained using the Chapman–Enskog theory [17].

Two different nonequilibrium chemistry models are used in the present work. For the convergent–divergent nozzle flow, an air dissociation/recombination chemistry model with five species (O_2, N_2, O, N, NO) and eleven elementary reaction steps [18] is adopted. For the dump combustor flow, an n-pentane-air chemistry model with five species (C_5H_{12}, O_2, N_2, CO_2, H_2O) and one global reaction step [19] is used.

2.2. *All-Mach-Number Formulation*

As noted earlier in the Introduction, the two main difficulties that render the compressible flow algorithms ineffective at low Mach numbers are the roundoff error caused by the singular pressure gradient term in the momentum equations (the pressure term is of order $1/M^2$ while the convective term is of order unity in the nondimensional momentum equations) and the stiffness caused by the wide disparities in eigenvalues. To circumvent the pressure singularity problem, we first note that it is the pressure gradient, not the actual pressure, that is involved in the momentum balance. Therefore, the pressure may be decomposed into a constant reference pressure part and a gauge pressure part as follows:

$$p(x, y, t) = p_0 + p_g(x, y, t). \tag{3}$$

To maximize the benefit of this measure, p_0 should be taken to comprise the majority of p. Physically, the gauge pressure p_g amounts to the dynamic pressure responsible for the velocity–pressure coupling in the momentum equation and is that part of pressure that drives the flow. With this representation of pressure, and noting that $\nabla(p_0+p_g)=\nabla p_g$, the static pressure p in the momentum equation is replaced using the gauge pressure p_g. With proper selection of p_0 (usually the freestream pressure or the upstream pressure), the magnitude of the pressure gradient term in the nondimensional momentum equations becomes of order unity as the Mach number approaches zero, and therefore the singularity is removed from the system.

In conventional compressible flow algorithms, pressure is not one of the dependent variables but it is calculated from the dependent variables and the equation of state. This is not a preferable approach at low Mach numbers, because roundoff errors are introduced in p and p_g, nullifying the pressure decomposition measure. To avoid contamination of the pressure field by the roundoff error, it is necessary to solve for p_g directly, i.e., to let p_g be one of the dependent variables. Following the approach by several researchers [5, 20, 21] in compressible flows and low Mach number flows, we add pseudo-time terms, composed of a set of primitive variables (p_g, u, v, h, Y_i), to the governing equations. The resulting Navier–Stokes equations are given in the nonconservative form (for simplicity, only 2D equations are presented)

$$\frac{1}{\beta}\frac{\partial p_g}{\partial \tau}+\frac{\partial \rho}{\partial t}+u\frac{\partial \rho}{\partial x}+\rho\frac{\partial u}{\partial x}+v\frac{\partial \rho}{\partial y}+\rho\frac{\partial v}{\partial y}=0, \tag{4a}$$

$$\rho\frac{\partial u}{\partial \tau}+\rho\frac{\partial u}{\partial t}+\rho u\frac{\partial u}{\partial x}+\rho v\frac{\partial u}{\partial y}+\frac{\partial p_g}{\partial x}=\frac{\partial \tau_{xx}}{\partial x}+\frac{\partial \tau_{xy}}{\partial y}, \tag{4b}$$

$$\rho\frac{\partial v}{\partial \tau}+\rho\frac{\partial v}{\partial t}+\rho u\frac{\partial v}{\partial x}+\rho v\frac{\partial v}{\partial y}+\frac{\partial p_g}{\partial y}=\frac{\partial \tau_{xy}}{\partial x}+\frac{\partial \tau_{yy}}{\partial y}, \tag{4c}$$

$$\rho\frac{\partial h}{\partial \tau}-\frac{\partial p_g}{\partial \tau}+\rho u\frac{\partial u}{\partial \tau}+\rho v\frac{\partial v}{\partial \tau}+\rho\frac{\partial H}{\partial t}+\rho u\frac{\partial H}{\partial x}+\rho v\frac{\partial H}{\partial y}-\frac{\partial p}{\partial t}=\frac{\partial(u\tau_{xx}+v\tau_{xy}+q_{x_e})}{\partial x}+\frac{\partial(u\tau_{xy}+v\tau_{yy}+q_{y_e})}{\partial y}, \tag{4d}$$

$$\rho\frac{\partial Y_i}{\partial \tau}+\rho\frac{\partial Y_i}{\partial t}+\rho u\frac{\partial Y_i}{\partial x}+\rho v\frac{\partial Y_i}{\partial y}=\frac{\partial q_{x_i}}{\partial x}+\frac{\partial q_{y_i}}{\partial y}+S_i, \tag{4e}$$

where τ is the pseudo time, h is the specific thermal enthalpy, and $H=h+\frac{1}{2}(u^2+v^2)$ is the total enthalpy of the gas mixture. Note that momentum, energy, and species equations keep their standard form, while only the continuity equation is modified by introducing the artificial compressibility method [21]. β in the continuity equation is a parameter for rescaling the eigenvalues of the new system of equations (to be discussed later). When steady state solutions are of interest, physical time terms can be dropped and only pseudo-time terms are retained.

In order to have better conservation properties and the ability to capture shock waves, we return to the conservative form by adding the continuity equation to the momentum, energy, and species equations in Eq. (4). The resulting Navier–Stokes equations in a conservative form in curvilinear coordinates are

$$\Gamma\frac{\partial \hat{\mathbf{Q}}}{\partial \tau}+\frac{\partial \tilde{\mathbf{Q}}}{\partial t}+\frac{\partial(\tilde{\mathbf{E}}-\tilde{\mathbf{E}}_v)}{\partial \xi}+\frac{\partial(\tilde{\mathbf{F}}-\tilde{\mathbf{F}}_v)}{\partial \eta}=\tilde{\mathbf{H}}, \tag{5}$$

where the primitive variable vector $\hat{\mathbf{Q}}$ and the preconditioning matrix Γ are given as

$$\hat{\mathbf{Q}}=\frac{y^\delta}{J}\begin{bmatrix} p_g \\ u \\ v \\ h \\ Y_1 \\ Y_2 \\ \vdots \\ Y_{N-1}\end{bmatrix},$$

$$\Gamma=\begin{bmatrix} 1/\beta & 0 & 0 & 0 & 0 & 0 & \cdot & \cdot & 0 \\ u/\beta & \rho & 0 & 0 & 0 & 0 & \cdot & \cdot & 0 \\ v/\beta & 0 & \rho & 0 & 0 & 0 & \cdot & \cdot & 0 \\ H/\beta-1 & \rho u & \rho v & \rho & 0 & 0 & \cdot & \cdot & 0 \\ Y_1/\beta & 0 & 0 & 0 & \rho & 0 & \cdot & \cdot & 0 \\ Y_2/\beta & 0 & 0 & 0 & 0 & \rho & 0 & \cdot & 0 \\ \vdots & \vdots & & \cdots & \cdot & 0 & \cdot & \cdot & 0 \\ & & \cdot & \cdot & \cdot & \cdot & 0 & \cdot & 0 \\ Y_{N-1}/\beta & 0 & 0 & \cdot & \cdot & \cdot & \cdot & 0 & \rho \end{bmatrix}.$$

The definitions of vectors $\tilde{\mathbf{Q}}$, $\tilde{\mathbf{E}}$, $\tilde{\mathbf{F}}$, $\tilde{\mathbf{E}}_v$, $\tilde{\mathbf{F}}_v$, and $\tilde{\mathbf{H}}$ in Eq. (5) are identical to those in Eq. (1) except that the absolute pressure in the momentum equations is replaced by the gauge pressure p_g.

The eigenvalues (in the ξ-direction) in the pseudo-time

can be obtained from the matrix $\Gamma^{-1}\mathbf{A}$, where $\mathbf{A}$ is the Jacobian $\partial\tilde{\mathbf{E}}/\partial\hat{\mathbf{Q}}$. The eigenvalues for a real gas are

$$\lambda = U, U, \frac{1}{2}\left[U\left(1+\frac{\beta}{c^2}\right) \pm \sqrt{U^2\left(1-\frac{\beta}{c^2}\right)^2 + 4\beta(\alpha_1^2+\alpha_2^2)}\right], U, U, \ldots, \quad (6)$$

where c is the speed of sound, $\alpha_1 = \xi_x$, $\alpha_2 = \xi_y$, and U is the contravariant velocity component defined as $U = \alpha_1 u + \alpha_2 v$. To obtain well-conditioned eigenvalues the scaling factor β is taken to be

$$\beta = u^2 + v^2;$$

then all the eigenvalues will have the same order of magnitude.

For convenience of presentation, the numerical scheme based on Eq. (5) will hereafter be referred to as the pressure-based scheme, while the schemes based on the standard form of equations (Eq. (1)) will be referred to as the density-based schemes.

3. NUMERICAL METHOD

3.1. *Dual Time-Stepping Integration Procedure*

To obtain time-accurate solutions for time-evolving problems, a dual time-stepping integration method is chosen. An implicit iterative procedure is used for asymptotic time-marching in pseudo-time. The solution converged in pseudo-time corresponds to a time-accurate solution in physical time. A similar technique has been used by Hosangadi *et al.* [15] and Rai [20]. One advantage of the dual time-stepping method is that the convergence of the iterative process is determined by the eigenvalue characteristics on the pseudo-time space and not by the original stiff eigenvalues.

A general dual-time marching procedure can be devised for Eq. (5) by using a three-level backward differencing for physical time, an Euler implicit differencing for pseudo-time, and a central differencing for space. The specific spatial difference method used in the present work may not be optimal for all cases (e.g., an upwind stencil may work better for high-speed flows), but it serves to illustrate the idea of the overall approach. The equation for the $(p+1)$th iteration in the pseudo-time at the $(n+1)$th level in physical time can be represented as

$$\Gamma\frac{\hat{\mathbf{Q}}^{p+1}-\hat{\mathbf{Q}}^{p}}{\Delta\tau} + \frac{a_1\tilde{\mathbf{Q}}^{p+1} + a_2\tilde{\mathbf{Q}}^{n} + a_3\tilde{\mathbf{Q}}^{n-1}}{\Delta t} + \frac{\partial(\tilde{\mathbf{E}}-\tilde{\mathbf{E}}_v)^{p+1}}{\partial\xi} + \frac{\partial(\tilde{\mathbf{F}}-\tilde{\mathbf{F}}_v)^{p+1}}{\partial\eta} = \tilde{\mathbf{H}}^{p+1}. \quad (7)$$

The coefficients a_1, a_2, and a_3 depend on the physical-time step and the level of temporal accuracy desired in physical time. In the case where the time step is constant and second-order accuracy is required, a_1, a_2, and a_3 can be chosen as

$$a_1 = \tfrac{3}{2}, \qquad a_2 = -2, \qquad a_3 = \tfrac{1}{2}.$$

It is noted that a higher order time accuracy can be easily obtained with negligible increase in computational time by using more time levels in the physical-time term in Eq. (7).

The dual-time marching method allows flexibility in selection of the time step sizes in the two time spaces. The physical-time step size Δt is determined based on the characteristic evolution of the unsteady flow under consideration. The pseudo-time step size $\Delta\tau$ is, on the other hand, determined based on the numerical stability of the algorithm and can be adjusted to give the optimum convergence rate for the pseudo-time iteration procedure. In the case that the steady-state solution is of interest, the physical-time term in Eq. (7) is eliminated. For test cases considered in the present work, pseudo-time CFL numbers between 5 to 10 are used in most calculations.

The terms at the $(p+1)$th time level in Eq. (7) need to be linearized for the construction of an implicit time marching scheme. The inviscid Jacobians used in the linearization are defined as

$$\mathbf{T} = \frac{\partial\tilde{\mathbf{Q}}}{\partial\hat{\mathbf{Q}}}, \qquad \mathbf{A} = \frac{\partial\tilde{\mathbf{E}}}{\partial\hat{\mathbf{Q}}}, \qquad \mathbf{B} = \frac{\partial\tilde{\mathbf{F}}}{\partial\hat{\mathbf{Q}}}.$$

The explicit expressions for $\mathbf{T}$, $\mathbf{A}$, and $\mathbf{B}$ are given in the Appendix. Following [5], with the definition of the differential operator

$$\mathbf{L}_v(\hat{\mathbf{Q}}) = \frac{\partial\tilde{\mathbf{E}}_v}{\partial\xi} + \frac{\partial\mathbf{F}_v}{\partial\eta}, \quad (8)$$

the viscous terms can be linearized as

$$\mathbf{L}_v(\hat{\mathbf{Q}})^{p+1} = \mathbf{L}_v(\hat{\mathbf{Q}})^{p} + \left(\frac{\partial}{\partial\xi}\mathbf{R}_{\xi\xi}\frac{\partial}{\partial\xi} + \frac{\partial}{\partial\xi}\mathbf{R}_{\xi\eta}\frac{\partial}{\partial\eta} + \frac{\partial}{\partial\eta}\mathbf{R}_{\eta\xi}\frac{\partial}{\partial\xi} + \frac{\partial}{\partial\eta}\mathbf{R}_{\eta\eta}\frac{\partial}{\partial\eta}\right)\Delta\hat{\mathbf{Q}}. \quad (9)$$

The viscous Jacobian matrices $\mathbf{R}_{\xi\xi}$, $\mathbf{R}_{\xi\eta}$, $\mathbf{R}_{\eta\xi}$, and $\mathbf{R}_{\eta\eta}$ can be obtained following a similar procedure as for the inviscid Jacobians.

3.2. *Chemical Source Term and Source Jacobian*

For a set of N_R elementary reactions involving N species, the reaction equations can be written in the general form

$$\sum_{j=1}^{N} v'_{ij} n_j \underset{k_{b_i}}{\overset{k_{f_i}}{\rightleftharpoons}} \sum_{j=1}^{N} v''_{ij} n_j, \qquad i = 1, 2, \ldots, N_R, \quad (10)$$

where v'_{ij} and v''_{ij} are the stoichiometric coefficients for species j appearing as a reactant in the ith forward and backward reactions, respectively, and n_j is the molar concentration for species j ($n_j = \rho Y_j / W_j$). Also, k_{f_i} and k_{b_i} are the forward and backward reaction rate constants for the ith reaction step, respectively. The reaction rate constant k_i (k_{f_i} or k_{b_i}) is given by the Arrhenius expression

$$k_i = A_i T^{m_i} e^{-E_i/R_u T}, \tag{11}$$

where E_i represents the activation energy, and A_i and m_i are constants.

From Eq. (11), the rate of change of mass concentration of species j is obtained by summing up the changes due to all reaction steps,

$$S_j = W_j \sum_{i=1}^{N_R} \left[(v''_{ij} - v'_{ij}) \left(k_{f_i} \prod_{l=1}^{N} n_l^{v'_{il}} - k_{b_i} \prod_{l=1}^{N} n_l^{v''_{il}} \right) \right]. \tag{12}$$

It is noted that, because of the vastly different time scales that may be involved in the elementary reactions and the flow, and the strong dependence of the source terms on temperature (exponentially) and density (ρ^2 or ρ^3, depending on the order of reaction), the set of equations may become very stiff for most flow conditions of interest. To mitigate this problem, chemical source terms are treated implicitly in the present work to improve numerical stability. Because of this implicit treatment, the attainable CFL numbers [illegible] implicit methods. As demonstrated in the nozzle flow calculations (see Numerical Test section), the same numerical efficiency is retained even when a large portion of the flow field is near chemical equilibrium where the chemistry is extremely stiff. Calculations using explicit chemistry (other terms in the governing equations were still treated implicitly) are also carried out for some of the test flows to examine the sensitivity of the reacting flow computation to the chemistry treatment. It is found that reduction of the CFL number by about three orders of magnitude is generally needed for numerical stability. The expression for chemistry source term Jacobian is provided in the Appendix; more details for the construction of the Jacobian can be found in [16].

3.3. *Discretized Equations*

After linearization, Eq. (7) can be expressed in the form

$$\left\{ \mathbf{\Gamma} - \Delta\tau\, \mathbf{D} + a_1 \frac{\Delta\tau}{\Delta t} \mathbf{T} + \Delta\tau \left(\frac{\partial \mathbf{A}}{\partial \xi} - \frac{\partial}{\partial \xi} \mathbf{R}_{\xi\xi} \frac{\partial}{\partial \xi} \right) + \Delta\tau \left(\frac{\partial \mathbf{B}}{\partial \eta} - \frac{\partial}{\partial \eta} \mathbf{R}_{\eta\eta} \frac{\partial}{\partial \eta} \right) \right\}^p \Delta\hat{\mathbf{Q}} = -\Delta\tau (\mathbf{R})^p, \tag{13}$$

where

$$\mathbf{R}^p = \frac{a_1 \tilde{\mathbf{Q}}^p + a_2 \tilde{\mathbf{Q}}^n + a_3 \tilde{\mathbf{Q}}^{n-1}}{\Delta t} + \frac{\partial (\tilde{\mathbf{E}} - \tilde{\mathbf{E}}_v)^p}{\partial \xi} + \frac{\partial (\tilde{\mathbf{F}} - \tilde{\mathbf{F}}_v)^p}{\partial \eta} - \tilde{\mathbf{H}}^p, \tag{14}$$

where $\mathbf{D} = \partial \tilde{\mathbf{H}} / \partial \hat{\mathbf{Q}}$ is the source term Jacobian. Central differences are used to discretize the spatial derivative terms in Eqs. (13) and (14) for both explicit and implicit operators. Note that in the implicit operator the cross-derivative viscous Jacobians are neglected. The resulting coupled algebraic equations are solved using a modified strongly implicit procedure (MSIP) originally proposed by Schneider and Zedan [22]. When Eq. (13) converges in the pseudo-time space at the $(n+1)$th physical time level, we obtain $\tilde{\mathbf{Q}}^{n+1} = \tilde{\mathbf{Q}}(\hat{\mathbf{Q}}^{p+1})$ and the right-hand side of Eq. (14) provides the time accurate solution. As noted earlier, the physical-time terms are neglected for steady flow problems.

The MSIP method converts the left-hand side operator to two, one upper and one lower, triangular operator matrices and inverts them in sequence [22]. By sweeping in the diagonal directions, i.e., the direction that $i + 2j$ increases or decreases, the inversion of the two implicit operators can be fully vectorized, avoiding the recursive procedure occuring in the tridiagonal system incurred by the popular ADI procedure. Since the size of the blocks in implicit operators [illegible] operators can be prohibitively expensive without vectorization.

A frequently used "frozen operator" technique may also be adopted to reduce the computational cost of performing sub-iterations in unsteady flow calculations. In this, the implicit (left-hand side) operator is frozen after the first iteration in the pseudo-time. For subsequent iterations, only the explicit (right-hand side) operator needs to be recalculated and the solution is obtained by a simple backward and forward substitution of the saved, inverted implicit operator. This "frozen operator" strategy is not used in the present work.

The running time of the present calculations, including integrating eight equations, calculating chemical source terms and thermophysical properties, is about 140 μs/grid point/time step on a CRAY-YMP computer, using the cft77 version 5 compiler.

4. NUMERICAL TEST

Numerical examples are selected to test the various features of the present algorithm, i.e., the ability to handle wide variations in Mach number, chemical reactions, and

unsteady flow. Only laminar flows are considered. Boundary conditions are treated implicitly for all the cases considered. Method of characteristics based boundary conditions [5] are used at inflow and ouflow boundaries. The no-slip, non-catalytic conditions, adiabatic or constant temperature, and a normal pressure gradient condition obtained from the normal momentum equation are specified at the walls. The symmetry conditions are applied at the centerline.

4.1. *Convergent–Divergent Nozzle Flow*

The model problem concerns the flow through a convergent–divergent nozzle. Two nozzle geometries are considered for contraction area ratios (AR) of 50 and 1000 and inflow Mach numbers around 0.011 and 0.0006, respectively. The AR = 50 case considers a two-dimensional nozzle, while the AR = 1000 case, an axisymmetric geometry. The Reynolds number based on the conditions at the throat is 2×10^6 for AR = 50 case and 3×10^6 for AR = 1000 case. The air upstream of the nozzle entrance is assumed to be in chemical equilibrium, with temperature at 5000 K and pressure 10 atm. As the dissociated air flows through the nozzle, recombination reactions take place due to the reduction in temperature. An air dissociation/recombination chemistry model with five species (O_2, N_2, O, N, NO) and eleven elementary reaction steps [18] is adopted.

The Mach number contours are plotted in Fig. 1 for the two cases. A 80×33 grid for AR = 50 and 150×38 grid for AR = 1000 are used with clustering near the wall. Figure 2 presents the Mach number, static pressure, temperature,

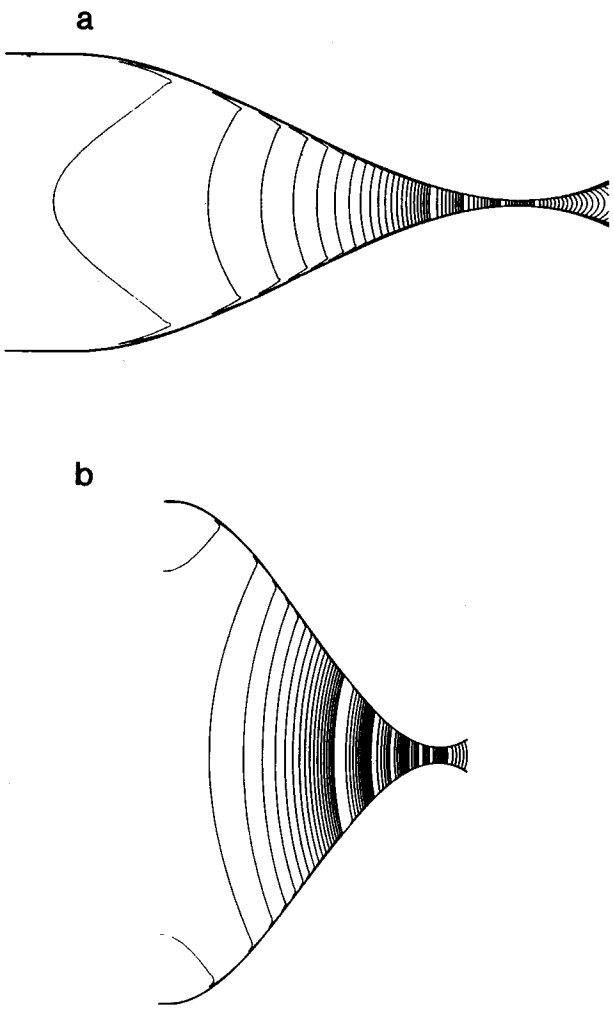

FIG. 1. Mach number contours for the convergent-divergent nozzle flows: (a) the 2D nozzle (AR = 50); (b) the axisymmetric nozzle (AR = 1000).

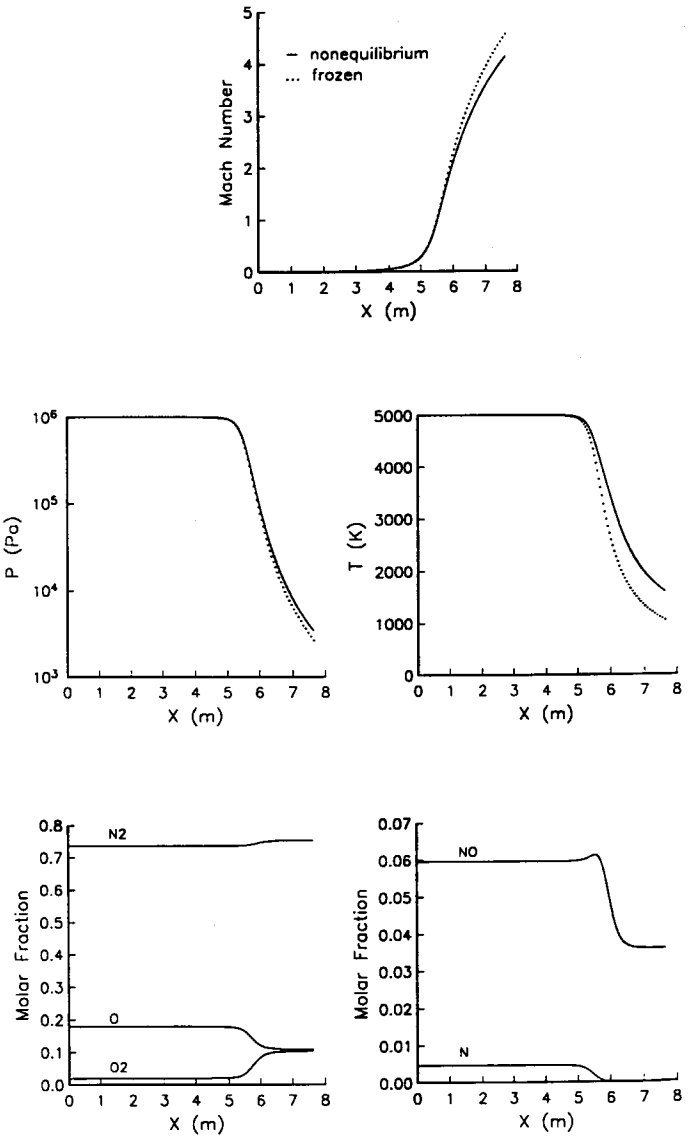

FIG. 2. Distribution of flow properties along the centerline of the 2D nozzle.

and species molar fractions along the nozzle centerline for the 2D nozzle (AR = 50). To illustrate the effects of non-equilibrium chemistry, results with frozen chemistry model are also presented for comparison. Because of the high temperature and pressure in the bulk of the subsonic section of the nozzle, chemical reactions are very close to equilibrium and the species molar fractions do not change significantly from their inflow values until close to the nozzle throat, where temperature and pressure undergo rapid changes caused by flow acceleration. Near the exit of the nozzle, chemical reactions become essentially frozen due to the relatively low temperature and pressure.

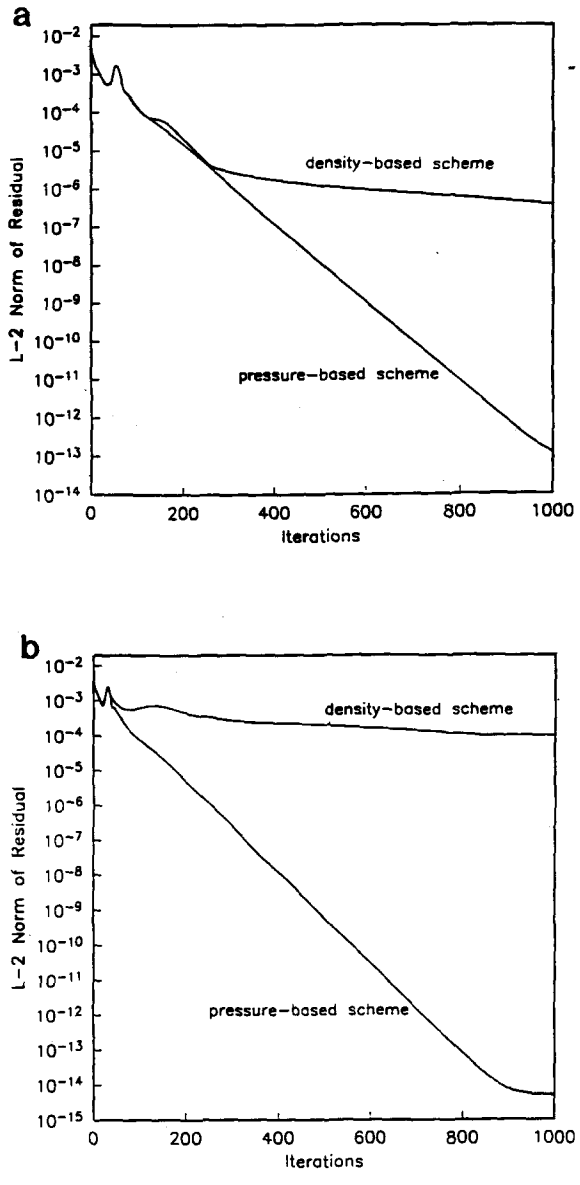

FIG. 3. Convergence histories for the convergent–divergent nozzle flow calculations: (a) the 2D nozzle (AR = 50); (b) the axisymmetric nozzle (AR = 1000).

The convergence histories of the two nozzle calculations are shown in Fig. 3 (results from the present method are labeled as pressure-based scheme). For comparison, results obtained using a density-based scheme are also presented. As expected, the convergence of the present scheme is very fast for both nozzle geometries although the inflow Mach numbers are quite low for the two cases. In contrast, the density-based scheme shows slow convergence in the AR = 50 case and very poor convergence in the AR = 1000 case.

As noted earlier, the chemistry becomes very stiff as chemical equilibrium is approached. However, because of the effectiveness of the implicit chemistry treatment, no difficulty was encountered in the present nozzle calculation despite a large portion of the flow being at or near chemical equilibrium.

4.2. *Dump Combustor Flow*

Two types of two-dimensional dump combustors, one symmetric and one asymmetric, are considered to study the capability of the present method for recirculating flows. The expansion ratios are 3.0 and 1.94 for the symmetric and asymmetric cases, respectively. Fully developed flow is assumed at the inlet plane for both cases. The computational domain starts at a distance upstream of the step and is extended far enough downstream for flow redevelopment. For the symmetric case, the inlet plane is located at $x/s = -3$ and the exit plane at $x/s = 12$. For the asymmetric

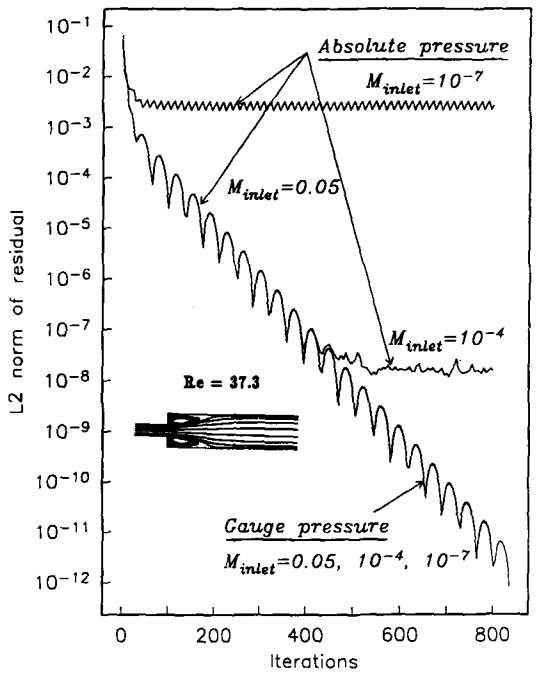

FIG. 4. Convergence history for the two-dimensional symmetric dump combustor flow (non-reacting), Re = 37.3.

case, the inlet and exit locations are at $x/s = -4$ and $x/s = 40$, respectively. Here s denotes the step height and x the streamwise distance.

For the symmetric case, only half of the domain is considered in the computation due to symmetry. The inlet Reynolds number based on the inlet bulk velocity and the step height is 37.3. A 51×29 grid is used with grid clustering near the wall and the step. A cold flow without combustion is studied for this configuration with a constant inlet and wall temperature of 300 K. Several inlet Mach numbers, ranging from 10^{-7} to 0.05, are considered to study the convergence properties for this flow. Also, the effect of using both absolute and gauge pressures on the convergence characteristics is examined. The convergence history is presented in Fig. 4. It shows that the convergence patterns are identical for the three Mach numbers, 10^{-7}, 10^{-4}, and 0.05, when the gauge pressure p_g is used as the dependent variable. However, if the absolute pressure p is chosen as the dependent variable, the convergence deteriorates as the inlet Mach number decreases. It fails to converge at all for the case with the inlet Mach number of 10^{-7}. The particle traces of the converged solution are also shown in the insert in Fig. 4. It clearly shows the presence of flow recirculation and reattachment behind the expansion step. For the present

which is in good agreement with the result by Tenpas and Pletcher ($x_r/s = 4.048$) [23].

Both non-reacting and reacting flows are considered for the asymmetric case. An n-pentane–air chemistry model with five species (C_5H_{12}, O_2, N_2, CO_2, H_2O) and one global reaction step [19] is used. For the reacting flow, the fuel is pre-mixed before it enters the combustor. The inlet temperature is 300 K and the wall is assumed adiabatic. An ignition source is placed near the eye of the corner recirculation zone to initiate the combustion. Two Reynolds numbers (based on the hydraulic diameter of the inlet (small) channel and the bulk velocity), 389 and 1000, are considered for this geometry. The inlet Mach number for this flow is 0.004. A 81×31 grid is used for both Reynolds numbers. Figure 5 shows velocity vectors and particle traces for both non-reacting and reacting flows at $\mathrm{Re} = 1000$. It is interesting to note that for the nonreacting flow case a second recirculation zone exists at the bottom wall across the main corner recirculation zone, consistent with the experimental observation by Armaly *et al.* [24]. The corner recirculation zone in the reacting flow is much diminished due to the gas expansion caused by combustion, and the second recirculation zone disappears in this case.

Figure 6 shows velocity profiles for the nonreacting flow case at some selected streamwise stations downstream of the step for both Reynolds numbers. The u_{max} in the figure is the maximum velocity at the inlet plane. The present numerical predictions agree very well with the experimental data in [24] for the $\mathrm{Re} = 389$ case. However, some discrepancies exist for the $\mathrm{Re} = 1000$ case, which may be attributed to the

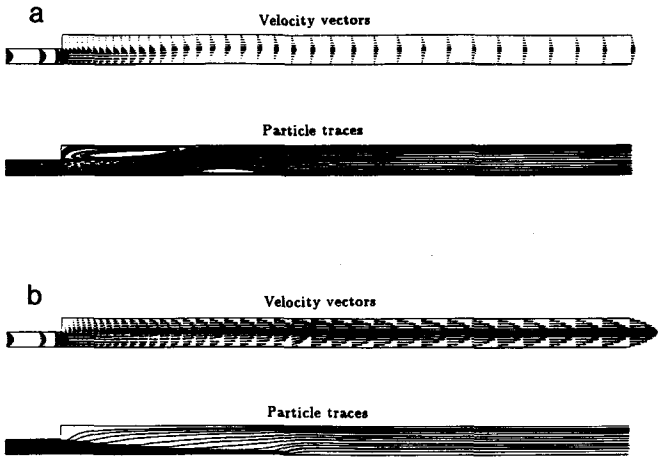

FIG. 5. Velocity vectors and particle traces for the two-dimensional asymmetric dump combustor flow at $\mathrm{Re} = 1000$: (a) non-reacting flow; (b) reacting flow.

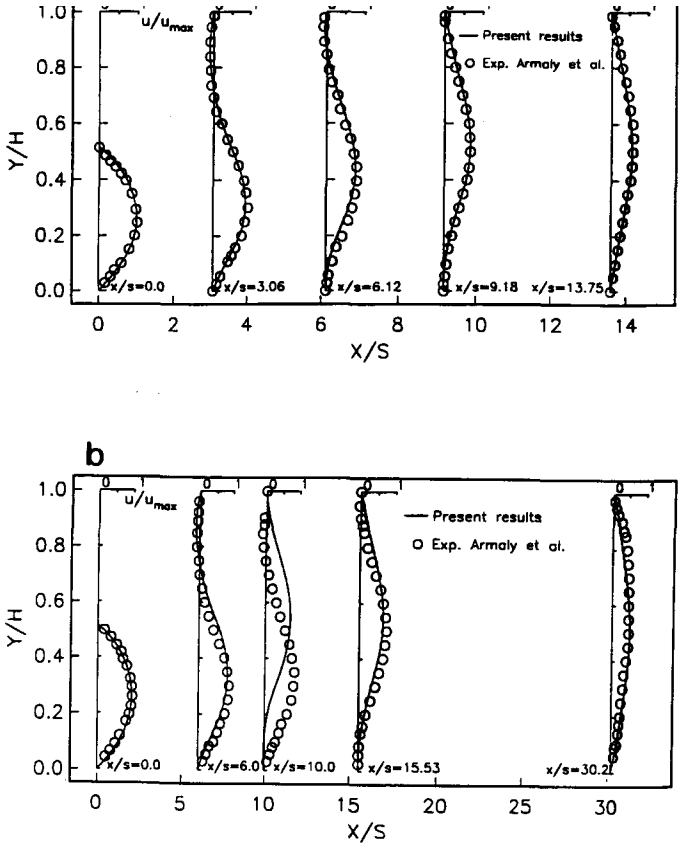

FIG. 6. Velocity profiles for the two-dimensional asymmetric dump combustor flow (non-reacting): (a) $\mathrm{Re} = 389$; (b) $\mathrm{Re} = 1000$.

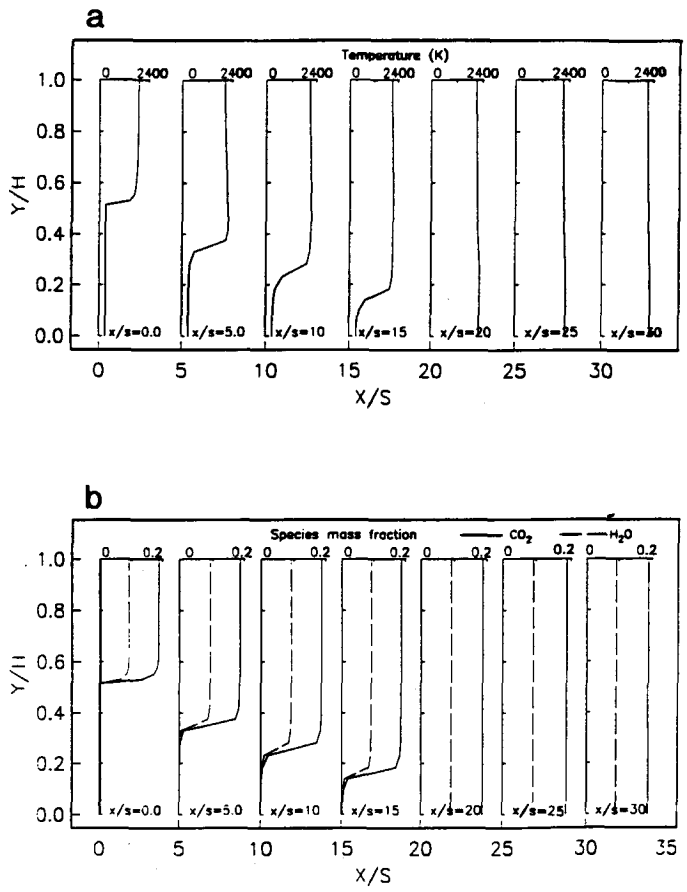

FIG. 7. Temperature and species distributions for the two-dimensional asymmetric dump combustor flow at Re = 1000 (reacting): (a) temperature; (b) species mass fraction.

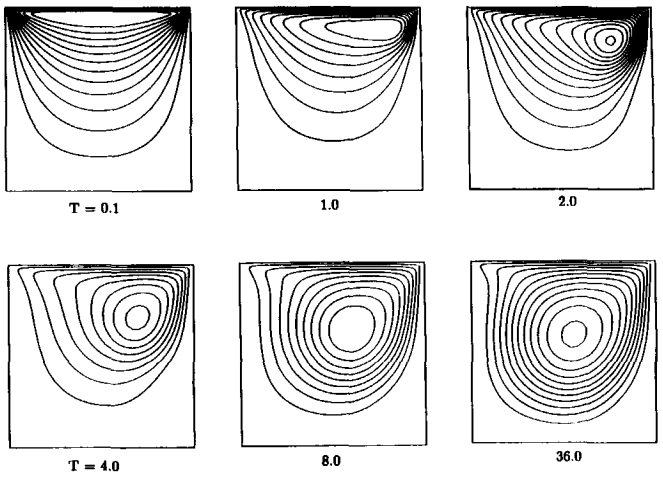

FIG. 8. Time history of streamfunction contours with impulsively started lid, Re = 400.

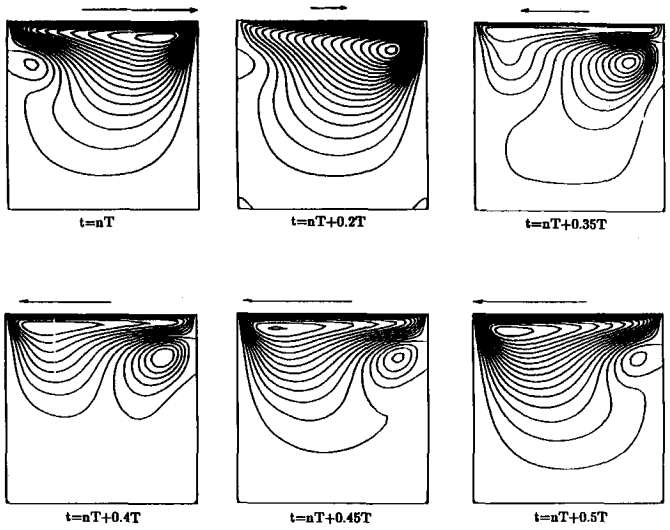

FIG. 9. Time history of streamfunction contours with oscillating lid, Re = 400.

presence of the second recirculation zone discussed earlier. Armaly *et al.* [24] reported that this second recirculation zone began to destroy the two dimensionality of the flow for Reynolds number above the value of 400 for thir test conditions. Figure 7 shows the temperature and combustion product mass fraction distributions at some selected streamwise stations for the reacting flow case. The discontinuities in the distributions mark the locations of the flame surface.

4.3. *Unsteady Driven Cavity Flow*

Two types of unsteady flow in a square cavity are considered here to study the unsteady capabilities of the present method. The first case considers the flow with an impulsively started lid. A 51 × 51 stretched grid is used. The Reynolds number based on the lid velocity and the length

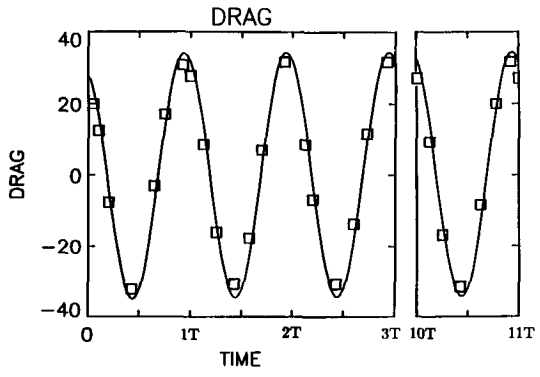

FIG. 10. Time history of drag coefficient on the oscillating lid, Re = 400 (———, present study; □, numerical solution by Soh and Goodrich [25]).

of the cavity is 400 and the Mach number is 10^{-5}. During the first few physical time steps, about 150 iterations are required to converge to a level of 5×10^{-5} (the initial residual is about 5×10^{-1}). As the solution develops in time, the number of iterations decreases rapidly and becomes one as the steady-state solution is approached.

Figure 8 shows streamlines at several non-dimensional time steps. The flows reaches steady state at around $T = 36$. The solution is verified by comparing the drag coefficient on the lid with that of Soh and Goodrich [25] and u and v velocity profiles at steady state with Ghio *et al.* [26]. Good agreement is observed in both cases, but this comparison is not presented here for reason of space.

The second case considers oscillatory flow in the cavity. The lid is subject to an oscillatory motion as described by $u = u_0 \cos(\omega t)$. The grid used and the Reynolds number (based on the maximum lid velocity) are identical to the impulsively started case. Forty time steps were used for each periodic cycle. The time integration is carried on until a periodic motion is observed in the flow. For the present case, it takes about 35 iterations at each physical time step to converge the residual to a level of 5×10^{-5}. About eight cycles are required to reach a periodic state in the flow.

Some selected streamfunction contours during the first half cycle at a periodic state are shown in Fig. 9. The results at the second half cycle are the mirror image of those at the first half cycle. The time history of the drag coefficient on the lid is again compared with that of Soh and Goodrich [25] in Fig. 10 and the agreement is very favorable.

CONCLUDING REMARKS

A time-accurate, coupled implicit procedure has been developed for solving the unsteady chemical non-equilibrium Navier–Stokes equations over a wide range of Mach numbers. The approach employs the strong conservative form of governing equations but uses primitive variables as primary dependent variables. This method has well-conditioned eigenvalues and pressure gradient terms at all Mach numbers and appears to be effective for the test cases considered, with Mach numbers ranging from 10^{-7} to about 4.2. Work for further algorithm validation and the implementation of a turbulence model is still needed and is being planned.

APPENDIX

The number of species equations is assumed to be five ($N = 5$) in the Jacobian matrices given below,

$$\mathbf{T} = \begin{bmatrix} \frac{1}{RT} & 0 & 0 & -\frac{\rho}{C_p T} & \rho\Omega_1 & \rho\Omega_2 & \rho\Omega_3 & \rho\Omega_4 \\ \frac{u}{RT} & \rho & 0 & -\frac{\rho u}{C_p T} & \rho u\Omega_1 & \rho u\Omega_2 & \rho u\Omega_3 & \rho u\Omega_4 \\ \frac{v}{RT} & 0 & \rho & -\frac{\rho v}{C_p T} & \rho v\Omega_1 & \rho v\Omega_2 & \rho v\Omega_3 & \rho v\Omega_4 \\ \frac{H}{RT} - 1 & \rho u & \rho v & \rho\left(1 - \frac{H}{C_p T}\right) & \rho H\Omega_1 & \rho H\Omega_2 & \rho H\Omega_3 & \rho H\Omega_4 \\ \frac{Y_1}{RT} & 0 & 0 & -\frac{\rho Y_1}{C_p T} & \rho\Theta_1 & \rho Y_1\Omega_2 & \rho Y_1\Omega_3 & \rho Y_1\Omega_4 \\ \frac{Y_2}{RT} & 0 & 0 & -\frac{\rho Y_2}{C_p T} & \rho Y_2\Omega_1 & \rho\Theta_2 & \rho Y_2\Omega_3 & \rho Y_2\Omega_4 \\ \frac{Y_3}{RT} & 0 & 0 & -\frac{\rho Y_3}{C_p T} & \rho Y_3\Omega_1 & \rho Y_3\Omega_2 & \rho\Theta_3 & \rho Y_3\Omega_4 \\ \frac{Y_4}{RT} & 0 & 0 & -\frac{\rho Y_4}{C_p T} & \rho Y_4\Omega_1 & \rho Y_4\Omega_2 & \rho Y_4\Omega_3 & \rho\Theta_4 \end{bmatrix}, \tag{A.1}$$

where

$$\Omega_i = -W\left(\frac{1}{W_i}-\frac{1}{W_N}\right)+\frac{(h_i-h_N)}{C_pT}, \qquad \Theta_i = 1+Y_i\Omega_i,$$

and W is the molecular weight of the gas mixture;

$$\mathbf{A}=\begin{bmatrix}
\frac{U}{RT} & \rho\alpha_1 & \rho\alpha_2 & -\frac{\rho U}{C_pT} & \rho U\Omega_1 & \rho U\Omega_2 & \rho U\Omega_3 & \rho U\Omega_4 \\
\alpha_1+\frac{uU}{RT} & \rho(U+u\alpha_1) & \rho u\alpha_2 & -\frac{\rho uU}{C_pT} & \rho uU\Omega_1 & \rho uU\Omega_2 & \rho uU\Omega_3 & \rho uU\Omega_4 \\
\alpha_2+\frac{vU}{RT} & \rho v\alpha_1 & \rho(U+v\alpha_2) & -\frac{\rho vU}{C_pT} & \rho vU\Omega_1 & \rho vU\Omega_2 & \rho vU\Omega_3 & \rho vU\Omega_4 \\
\frac{UH}{RT} & \rho(H\alpha_1+uU) & \rho(H\alpha_2+vU) & \rho U\phi & \rho UH\Omega_1 & \rho UH\Omega_2 & \rho UH\Omega_3 & \rho UH\Omega_4 \\
\frac{UY_1}{RT} & \rho Y_1\alpha_1 & \rho Y_1\alpha_2 & -\frac{\rho UY_1}{C_pT} & \rho U\Theta_1 & \rho UY_1\Omega_2 & \rho UY_1\Omega_3 & \rho UY_1\Omega_4 \\
\frac{UY_2}{RT} & \rho Y_2\alpha_1 & \rho Y_2\alpha_2 & -\frac{\rho UY_2}{C_pT} & \rho UY_2\Omega_1 & \rho U\Theta_2 & \rho UY_2\Omega_3 & \rho UY_2\Omega_4 \\
\frac{UY_3}{RT} & \rho Y_3\alpha_1 & \rho Y_3\alpha_2 & -\frac{\rho UY_3}{C_pT} & \rho UY_3\Omega_1 & \rho UY_3\Omega_2 & \rho U\Theta_3 & \rho UY_3\Omega_4 \\
\frac{UY_4}{RT} & \rho Y_4\alpha_1 & \rho Y_4\alpha_2 & -\frac{\rho UY_4}{C_pT} & \rho UY_4\Omega_1 & \rho UY_4\Omega_2 & \rho UY_4\Omega_3 & \rho U\Theta_4
\end{bmatrix}, \tag{A.2}$$

where

$$U=\alpha_1 u+\alpha_2 v, \qquad \alpha_1=\xi_x, \qquad \alpha_2=\xi_y,$$

and

$$\phi = 1-\frac{H}{C_pT}.$$

The Jacobian matrix $\mathbf{B}$ is obtained by letting $\alpha_1=\eta_x$, $\alpha_2=\eta_y$.

The chemical source term Jacobian has the general form

$$\mathbf{D}^C=\begin{bmatrix}
0 & 0 & 0 & 0 & 0 & 0 & 0 & 0 \\
0 & 0 & 0 & 0 & 0 & 0 & 0 & 0 \\
0 & 0 & 0 & 0 & 0 & 0 & 0 & 0 \\
0 & 0 & 0 & 0 & 0 & 0 & 0 & 0 \\
\frac{\partial S_1}{\partial p_g} & \frac{\partial S_1}{\partial u} & \frac{\partial S_1}{\partial v} & \frac{\partial S_1}{\partial h} & \frac{\partial S_1}{\partial Y_1} & \frac{\partial S_1}{\partial Y_2} & \frac{\partial S_1}{\partial Y_3} & \frac{\partial S_1}{\partial Y_4} \\
\frac{\partial S_2}{\partial p_g} & \frac{\partial S_2}{\partial u} & \frac{\partial S_2}{\partial v} & \frac{\partial S_2}{\partial h} & \frac{\partial S_2}{\partial Y_1} & \frac{\partial S_2}{\partial Y_2} & \frac{\partial S_2}{\partial Y_3} & \frac{\partial S_2}{\partial Y_4} \\
\frac{\partial S_3}{\partial p_g} & \frac{\partial S_3}{\partial u} & \frac{\partial S_3}{\partial v} & \frac{\partial S_3}{\partial h} & \frac{\partial S_3}{\partial Y_1} & \frac{\partial S_3}{\partial Y_2} & \frac{\partial S_3}{\partial Y_3} & \frac{\partial S_3}{\partial Y_4} \\
\frac{\partial S_4}{\partial p_g} & \frac{\partial S_4}{\partial u} & \frac{\partial S_4}{\partial v} & \frac{\partial S_4}{\partial h} & \frac{\partial S_4}{\partial Y_1} & \frac{\partial S_4}{\partial Y_2} & \frac{\partial S_4}{\partial Y_3} & \frac{\partial S_4}{\partial Y_4}
\end{bmatrix}, \tag{A.3}$$

where

$$\frac{\partial S_j}{\partial p_g}=\frac{1}{RT}\frac{\partial S_j}{\partial \rho},$$

$$\frac{\partial S_j}{\partial u}=\frac{\partial S_j}{\partial v}=0,$$

$$\frac{\partial S_j}{\partial h}=\frac{1}{C_p}\left(\frac{\partial S_j}{\partial T}-\frac{\rho}{T}\frac{\partial S_j}{\partial \rho}\right),$$

$$\frac{\partial S_j}{\partial Y_i}=W_j\sum_{k=1}^{N_R}\left[(v''_{kj}-v'_{kj})\left(v'_{ki}\frac{k_{f_k}}{Y_i}\prod_{l=1}^{N}n_l^{v'_{kl}}-v''_{ki}\frac{k_{b_k}}{Y_i}\prod_{l=1}^{N}n_l^{v''_{kl}}\right)\right]$$
$$-\rho\left[W\left(\frac{1}{W_i}-\frac{1}{W_N}\right)-\frac{(h_i-h_N)}{C_pT}\right]\frac{\partial S_j}{\partial \rho}-\frac{(h_i-h_N)}{C_p}\frac{\partial S_j}{\partial T},$$

and

$$\frac{\partial S_j}{\partial \rho}=W_j\sum_{i=1}^{N_R}\left((v''_{ij}-v'_{ij})\left[\frac{k_{f_i}}{\rho}\left(\sum_{l=1}^{N}v'_{il}\right)\prod_{l=1}^{N}n_l^{v'_{il}}-\frac{k_{b_i}}{\rho}\left(\sum_{l=1}^{N}v''_{il}\right)\prod_{l=1}^{N}n_l^{v''_{il}}\right]\right),$$

$$\frac{\partial S_j}{\partial T}=W_j\sum_{i=1}^{N_R}\left((v''_{ij}-v'_{ij})\left[\frac{k_{f_i}}{T}\left(m_{f_i}+\frac{E_{f_i}}{R_uT}\right)\prod_{l=1}^{N}n_l^{v'_{il}}-\frac{k_{b_i}}{T}\left(m_{b_i}+\frac{E_{b_i}}{R_uT}\right)\prod_{l=1}^{N}n_l^{v''_{il}}\right]\right).$$

REFERENCES

1. W. R. Briley, H. McDonald, and S. J. Shamroth, *AIAA J.* **21**, 1467 (1983).
2. C. L. Merkle and D. Choi, *AIAA J.* **23**, 1518 (1985).
3. E. Turkel, *J. Comput. Phys.* **72**, 277 (1987).
5. Y. H. Choi and C. L. Merkle, *J. Comput. Phys.*, to appear.
6. E. S. Oran and J. P. Boris, *Prog. Energy Combust. Sci.* **7**, 1 (1981).
7. J. Guerra and B. Gustafsson, *J. Comput. Phys.* **63**, 377 (1986).
8. G. Patnaik, R. H. Guirguis, J. P. Boris, and E. S. Oran, *J. Comput. Phys.* **71**, 1 (1987).
9. J. D. Ramshaw, P. J. O'Rourke, and L. R. Stein, *J. Comput. Phys.* **58**, 361 (1985).
10. K. H. Chen and R. H. Pletcher, *AIAA J.* **29**, 1241 (1991).
11. J. S. Shuen and S. Yoon, *AIAA J.* **27**, 1752 (1989).
12. G. V. Candler and R. W. MacCormack, AIAA Paper 88-511, 1988 (unpublished).
13. D. R. Eklund, J. P. Drummond, and H. A. Hassan, *AIAA J.* **28**, 1633 (1990).
14. A. A. Amsden, P. J. O'Rourke, and T. D. Butler, LA-11560-MS, Los Alamos National Laboratory, 1989 (unpublished).
15. A. Hosangadi, C. L. Merkle, and S. R. Turns, *AIAA J.* **28**, 1473 (1990).
16. J. S. Shuen, *J. Comput. Phys.* **99**, 233 (1992).
17. R. C. Reid, J. M. Prausnitz, and B. E. Poling, *The Properties of Gases and Liquids*, 4th ed. (McGraw–Hill, New York, 1988).
18. M. G. Dunn and S. W. Kang, NASA CR-2232, 1973 (unpublished).
19. C. K. Westbrook and F. L. Dryer, *Combust. Sci. Technol.* **27**, 31 (1981).
20. M. M. Rai, AIAA Paper 87-547, 1987 (unpublished).
21. A. J. Chorin, *J. Comput. Phys.* **2**, 12 (1967).
22. G. E. Schneider and M. Zedan, *Numer. Heat Transf.* **4**, 10 (1981).
23. P. W. TenPas and R. H. Plecther, *AIAA J.* **29**, 219 (1991).
24. B. F. Armaly, F. Durst, C. F. Pereira and B. Schonung, *J. Fluid Mech.* **127**, 473 (1983).
25. W. Y. Soh and J. W. Goodrich, *J. Comput. Phys.* **79**, 113 (1988).
26. U. Ghia, K. N. Ghia, and C. T. Shin, *J. Comput. Phys.* **48**, 387 (1982).